https://doi.org/10.1016/j.electacta.2017.11.134

A microfluidic all-vanadium photoelectrochemical cell for solar energy storage

Xiaohong Jiao[a,b], Rong Chen[a,b]*, Xun Zhu[a,b], Qiang Liao[a,b], Dingding Ye[a,b], Biao Zhang[a,b], Liang An[c], Hao Feng[a,b], Wei Zhang[a,b]

[a] Key Laboratory of Low-grade Energy Utilization Technologies and Systems (Chongqing University), Ministry of Education, Chongqing 400030, China

[b] Institute of Engineering Thermophysics, Chongqing University, Chongqing 400030, China

[c] Department of Mechanical Engineering, The Hong Kong Polytechnic University, Hung Hom, Kowloon, Hong Kong, China

*Corresponding author:

[a,b] Tel.: 0086-23-65103119; fax: 0086-23-65102474; e-mail: rchen@cqu.edu.cn (Rong Chen)

Abstract

In this work, a microfluidic all-vanadium photoelectrochemical cell (μVPEC) was designed for the solar energy storage. The miniaturization design could enhance the photon and mass transport, reduce the internal cell resistance, and improve the uniformity of the light distribution. Because of these advantages, the developed μVPEC was able to yield good performance. Experimental results indicated that the developed μVPEC showed good photoresponse and operation stability. Besides, its performance was also evaluated under various operating conditions, including the membrane thickness, the light intensity and the vanadium ion concentrations. It was shown that although the vanadium ion permeation was small with thicker membrane, the increased proton transfer resistance decreased the photocurrent density. The increase of the light intensity could produce more photo-generated electron-hole pairs, which could improve the photoelectrochemical reaction rate and the conversion rate.

It was also found that the photocurrent density was increased with the vanadium ion concentration as a result of the enhanced mass transfer. The results obtained in this work reveal that the developed all-vanadium photoelectrochemical cell shows the promising potential for the solar energy storage.

Keywords**:** Microfluidic all-vanadium photoelectrochemical cell; Solar energy storage; Photocurrent density; Conversion rate

1 Introduction

Owing to the grand challenge of energy crisis, the replacement of fossil fuels by renewable energy becomes inevitable to ensure the sustainable development. To date, a considerable number of researchers have devoted their efforts to the development of renewable energy, including the solar energy, wind energy and tidal energy, etc [1-4]. Solar energy, as one of main renewable energy resources, has attracted wide attention of the researchers because it is clean, extensive and inexhaustible [5]. Presently, main commercial solar energy utilizations rely on the photothermal and photoelectric conversions by converting the solar energy into heat and electricity, respectively [6-7]. However, both solar utilization technologies face the problem of the intermittence. Hence, the energy storage is usually required in these applications.

Typically, the common methods for the energy storage during the solar energy utilization processes include the solar-thermal energy storage, electrochemical energy storage and photochemical energy storage [8-12]. Among them, vanadium redox flow battery (VRB), proposed by Maria Skyllas-Kazacos and co-workers in 1985, has been regarded as one of the most competitive candidates for large-scale energy storage [13-15]. The VRB can offer lots of advantages, such as long life cycle, large storage capacity, high efficiency and safety [16-17]. Moreover, the electrolyte metal ions are all vanadium, which can effectively avoid the cross contamination in the electrolyte solution and be easily recycled [18-19]. In recent, Liu and his co-authors combined the photoelectrochemical cell with the vanadium redox flow battery to construct a

photoelectrochemical vanadium redox battery for solar energy storage [20-23]. This method can directly convert the solar energy into the chemical energy via the photoelectrochemical reactions. However, there are still some drawbacks in their designs. For example, they used the batch reactor design instead of continuous flow mode. Large-scale reactors not only result in large internal resistance between the electrodes but also increase the photon and mass transport, which inhibits the reaction rate and energy conversion efficiency. Besides, the photoanode in their system was prepared by directly depositing the TiO_2 on the FTO glass using a doctor blade. The resultant poor connection between the TiO_2 film and FTO glass caused relatively low electron transfer, which may be unfavorable for preventing the recombination of the photo-excited electron-hole pairs.

In recent, the incorporation of microfluidics into the reactor design has been widely used in the photoreactors [24-27], because microfluidics has large surface-to-volume ratio to enhance the mass and photon transfer. Moreover, because of the microreactor design, the light distribution can be more uniform. Besides, previous works have also demonstrated that the addition of a compact TiO_2 layer between the porous TiO_2 layer and the conductive substrate could not only ensure the strong adhesion of the TiO_2 film to the conductive substrate but also provide high conductivity to prevent the recombination of the photo-excited electron-hole pairs, while the top porous TiO_2 layer could still provide sufficient path for the mass and photon transport and large specific surface area for the photoelectrochemical reactions [11, 28-30]. All these

merits are beneficial for the improvement in the photoelectrochemical reaction rate and conversion efficiency. In line with this idea, a microfluidic all-vanadium photoelectrochemical cell (μVPEC) was proposed for the solar energy storage in the present work. The morphology and chemical composition of the photoanode were characterized using the FESEM and XRD. The performance of the developed μVPEC was also evaluated under various design and operating parameters, including the thickness of the proton exchange membrane, the light intensity as well as the vanadium ion concentration.

2 Experimental

2.1 Preparation of the electrolyte

Prior to the experiment, the photoanode and cathode electrolytes were firstly prepared. The photoanode electrolyte was prepared by dissolving a certain amount of vanadium (IV) sulfate oxide hydrate ($VOSO_4 \cdot xH_2O$) (99.9%, Sigma-Aldrich, USA) in 2.0 M H_2SO_4. In this work, three photoanode electrolytes with the VO^{2+} concentration ranging from 10.0 mM, 50.0 mM to 100.0 mM were prepared. For the cathode electrolyte, a certain amount of V_2O_3 powder (95%, Alfa Aesar, USA) was firstly dissolved in 200 mL 5.0 M H_2SO_4 aqueous solution via the evaporation reflux at a temperature of 120 °C in a magnetic stirring oil batch. After all the powders was dissolved, the prepared solution was cooled down to room temperature. Distilled water was then added into the prepared solution to maintain the H_2SO_4 concentration at 2.0 M, which was the same as the photoanode electrolyte. Similarly, three

corresponding cathode electrolytes with the V^{3+} concentrations of 10.0 mM, 50.0 mM and 100.0 mM were prepared.

2.2 Fabrication of the photoanode

In this work, the photoanode was formed by depositing the TiO_2 film on the FTO glass (resistance 10 Ω per square, Meijingyuan Technology Co., China). The TiO_2 film was consisted of two layers. One was the dense layer at the bottom, the other was the top porous layer. The detailed preparation procedure is presented as follows. First of all, the FTO conducting glass was cleaned by sonication in acetone, isopropanol and ethanol mixture solution with the volume ratio of 1:1:1. The cleaned FTO conducting glass was then washed with distilled water followed by the drying in an oven for 8 h at 80 °C. After cleaning, the bottom dense layer coated onto the FTO conducting glass was formed by the spin-coating method using the densely packed TiO_2 layer sol (Kunshan Sunlaite New Energy Technology Co., China). Here, 0.01 mL densely packed TiO_2 layer sol was spun onto the FTO glass by the spin coater with a speed of 1000 rmp for 18 s and 3000 rmp for 30s subsequently. After that, the FTO glass coated with the TiO_2 sol was placed into a tube furnace and calcined at 500 °C for 0.5 h with the temperature rise rate of 10 °C/min to form the bottom dense layer. The top porous layer was prepared by the wet spraying method. In this step, 12 g TiO_2 nanoparticles (Aeroxide P25, Acros, Belgium) were firstly added into a mixture solution consisting of 120 mL DI water and 0.4 mL acetylacetone (Sigma-Aldrich, USA) with magnetic stirring. Then 0.2 mL of a Triton X-100

(Sigma-Aldrich, USA) was added to facilitate the spreading of the colloid. Afterwards, 2.4 g polyethylene glycol (Aladdin, China) was added. The solution was then mixed for 12 hours with magnetic stirring. The prepared colloid was sprayed onto the dense layer by a spray gun and finally calcined at 550 °C for 2 hours with the temperature rise rate of 10 °C/min to form the top porous TiO_2 layer. The coated area was about 1.0 × 1.0 cm^2 and the final loading of TiO_2 was about 3.0 mg/cm^2.

2.3 Assembly and experimental setup

As schematically shown in Fig. 1a, The μVPEC was consisted of a photoanode, two reaction microchambers separated by a Nafion membrane, a cathode and a cover plate, which were assembled together by bolts. The photoanode and cathode had one inlet and one outlet, respectively. The triangular shape inlets and outlets were designed to ensure that the supplied liquid could be uniformly distributed on the entire electrodes. The depth of the reaction microchambers was 500 μm, which can greatly reduce the internal resistance of the cell and promote the mass transport. The commercial cathode of the Pt coated carbon paper (DMFC Cathode, Alfa Aesar, Great Britain) with the active area of 1.0 × 1.0 cm^2 was chosen as the cathode. The loading of Pt was about 1.0 mg/cm^2.

The schematic diagram of the experimental system is shown in Fig. 1b. As seen, it was consisted of a syringe pump (LSP04-1A, Longer, China), a 300-W Xe lamp (CEL-HXF300, Beijing Zhongjiaojinyuan technology company, China), a data collecting instrument (34972A, Angilet, America), two liquid containers and a

μVPEC. During the operation, the photoanode and cathode electrolyte solutions were introduced into the cell by the syringe pump. The Xe lamp provided the illumination to the μVPEC. The light intensity was controlled by adjusting the distance between the lamp and μVPEC, and measured by the visible radiometer (FZ-Z, Photoelectric Instrument Factory of Beijing Normal University, China). The photocurrent was recorded by the data collecting instrument.

3 Results and discussion

3.1 Working principle of μVPEC

During the working process, the photoanode and cathode electrolytes were continuously supplied into the reaction microchambers, respectively. Upon illumination, the photo-excited electron-hole pairs were generated in the TiO_2 photoanode as follows,

$$TiO_2 + h\nu \rightarrow TiO_2\ (e^- + h) \quad (1)$$

Because the photo-generated holes have strong oxidation ability, the vanadium ions VO^{2+} could be oxidized to VO_2^+,

$$VO^{2+} + H_2O + h \rightarrow VO_2^+ + e^- + 2H^+ \quad (2)$$

Then the generated electrons went through the external circuit to the cathode, at which V^{3+} captured the electrons to be reduced to V^{2+}.

$$V^{3+} + e^- \rightarrow V^{2+} \quad (3)$$

The generated protons crossed the Nafion membrane to complete a circuit. As such, the solar energy can be stored in the form of the highest and lowest valence states of the vanadium ions.

3.2 Characterization of the photoanode

To obtain the morphology of the prepared photoanode on the FTO conducting glass, the field emission scanning electron microscope (FESEM, S4800, Hitachi, Japan) was used. The results are shown in Fig. 2. Figs. 2a and 2b show the top view and cross-sectional view of the bottom dense layer, respectively. As can be seen, the bottom dense layer was compactly and uniformly adhered on the FTO conducting glass with a thickness of about 120 nm. Such thin and compact structure can not only provide a good contact and adhesion to the FTO conducting glass but also promote the electron transport. Figs. 2c and 2d show the top view and cross-sectional view of the top porous layer. It can be found that the TiO_2 nanoparticles were uniformly distributed on the bottom dense layer with numerous pores. This porous structure not only provides large specific surface area for the photoelectrochemical reactions but also offers plenty of path for the mass and photon transport. Besides, an X-ray diffraction was also used for the characterization of the crystalline phase of the fabricated photoanode, and the results are shown in Fig. 3. From the results, two crystalline phases of anatase-TiO_2 and rutile-TiO_2 could be observed.

3.3 Photoresphonse of the photoanode

The photoresponse of the photoanode to the illumination is an important factor to reflect the performance of the developed μVPEC. As a result, the photocurrent-time was characterized to study the photoresponse of the photoanode under the light on/off mode. In this section, the vanadium concentrations of both the photoanode and

cathode electrolytes were 100.0 mM, the flow rates at both the photoanode and cathode were set at 50 μL/min and the light intensity was kept at 130 mW/cm^2. Fig. 4 shows the photoresponse behavior under the light on/off mode. As can be seen, when the light was on, the photocurrent density was instantly boosted to about 0.075 mA/cm^2 with a relatively stable value during the light-on stage. When the light was turned off, the photocurrent density immediately dropped down to about zero. In the tested five cycles, the photoanode could well repeatedly respond to the illumination. This fact indicates that the photoanode has good photoresponse performance.

3.4 Effect of the Nafion membrane thickness

During the working process, the protons need to permeate through the proton exchange membrane to complete the circuit. Besides, the vanadium ions may also transport through the membrane. In this case, the transport of the proton and vanadium ion through the membrane can affect the performance of the developed μVPEC. Therefore, the membrane thickness is one of the most important parameters affecting the cell performance. In this work, three proton exchange membranes (Nafion 212 with the thickness of about 50 μm, Nafion 115 with the thickness of about 127 μm and Nafion 117 with the thickness of about 183 μm) were investigated to shed light on its influence. Actually, the membrane thickness effect on the proton transfer has been widely studied in the proton exchange membrane fuel cells and direct methanol fuel cells. It is revealed that large membrane thickness will increase the proton transfer resistance and thereby the internal cell resistance. Hence, we

mainly visited the effect of the membrane thickness on the vanadium ion permeation through the proton exchange membrane. To do this, the permeation ratio of VO^{2+} through the membrane was studied without illumination. The photoanode electrolyte with the VO^{2+} concentration of 100.0 mM and the cathode electrolyte of 2.0 M H_2SO_4 without vanadium were circulated in the developed μVPEC for 6 hours, respectively. The flow rates at both the electrodes were 50 μL/min. The collected electrolyte at the cathode outlet was then detected using an UV-Vis spectrophotometer to determine the VO^{2+} concentration, which could then be utilized to estimate the VO^{2+} permeation ratio. The results are shown in Fig. 5a. As seen from the embedded figure in Fig. 5a, there existed a peak at the wavelength of about 760 nm, which could be assigned to VO^{2+} [31-33]. This fact implied that this method could be employed to quantitatively determine the VO^{2+} concentration at the cathode. With this result, the VO^{2+} permeation ratio under various membrane thicknesses could then be estimated by the following equation,

$$P = A / A_0 \tag{4}$$

where P is the VO^{2+} permeation ratio, A is the absorbance of the VO^{2+} at the cathode and A_0 is the absorbance of the VO^{2+} at the concentration of 100.0 mM.

As shown in Fig. 5, the permeation ratio of the VO^{2+} ion was gradually decreased with the increase of the membrane thickness. It is easy to understand that thinner membrane can decrease the vanadium transfer resistance, making it easy for the vanadium ion across the membrane and thereby large permeation ratio. It should be

pointed out that the difference in the VO^{2+} permeation ratio between these membranes was not significant. When the membrane thickness was increased from 50 μm to 183 μm, although it was more than two times higher, the permeation ratio was just decreased about 20%. The possible reason might be that the vanadium ion size is larger as compared to the protons, which made it not easy for the vanadium ions to permeate through the membrane. On the other hand, the protons can still easily permeate through the membrane so that the membrane thickness effect might mainly contribute to the proton transfer in the developed μVPEC. Afterwards, the effect of the membrane thickness on the performance of the developed μVPEC was studied under the illumination of 130 mW/cm^2. The concentrations of both V^{3+} and VO^{2+} were 100.0 mM and the flow rates were all 50 μL/min. Fig. 5b shows the cell performances of the developed μVPECs with various membranes. As can be seen, although the increase in the membrane thickness could reduce the vanadium ion permeation, the performance still decreased as the membrane thickness increased. The average photocurrent density of the Nafion 212 was about 0.097 mA/cm^2, which was higher than the Nafion 115 of about 0.076 mA/cm^2 and the Nafion 117 of 0.071 mA/cm^2. Clearly, this is because thinner membrane reduced the proton transfer resistance, which caused the reduction of the internal cell resistance and then increased the photocurrent density. In brief, although thicker membrane can reduce the vanadium ion permeation, which benefited for the improvement of the efficiency and capacity, the resultant increase of the proton transfer resistance leads to lowered performance in the present study. Hence, the development of the membrane with high

proton conductivity and low vanadium ion permeation is necessary in the future.

In addition, to demonstrate that the microreactor design can reduce the internal cell resistance as compared to the large-scale batch reactor, the electrochemical impedance spectroscopy (EIS) was conducted using an electrochemical workstation (Zahner, Germany) in a two-electrode testing system with the frequency swept from 100 kHz to 10 mHz and a perturbation of 10 mV. For comparison, we designed and fabricated a large-scale all-vanadium photoelectrochemical cell with the batch reactor design with the same active surface area and the Nafion 115 membrane. The distance between the photoanode and cathode was about 4.0 cm. The EIS measurements of both the batch reactor and the μVPEC were performed under illumination with the light intensity of 130 mW/cm^2. The vanadium concentration of both the photoanode and cathode electrolytes were 100.0 mM. The electrolytes in the batch reactor were static, while the electrolytes in the μVPEC were continuously supplied with the flow rates of 50 μL/min. The EIS Nyquist plots of the developed μVPEC and large-scale batch reactor are compared in Fig. 6. As seen, the impedance of the developed μVPEC was much smaller than that of the large-scale batch reactor at high frequency region because of the miniaturization design. This fact indicates that the internal cell resistance can be reduced by the microreactor design proposed in this work.

3.5 Effect of the light intensity

As mentioned above, the conversion of the solar energy into the chemical energy is

completed by the photoelectrochemical reactions, which is actuated by the light illumination. Hence the light intensity plays an important role in the performance. Because of this, the effect of the light intensity was studied in this section. Here, the concentrations of VO^{2+} and V^{3+} were kept at 100.0 mM, the flow rates were maintained at 50 μL/min, and the Nafion 115 membrane was chosen. The light intensity varied from 70 to 160 mW/cm^2. Fig. 7a shows the variation of the photocurrent density with the light intensity under the long-term operation of 6 hours. As can be seen in Fig. 7a, the average photocurrent density was increased from about 0.038 mA/cm^2 to about 0.086 mA/cm^2 as the light intensity was increased from 70 to 160 mW/cm^2. It is easy to understand that increasing the light intensity can generate more photo-excited electron-hole pairs, leading to more vanadium ions to be oxidized and thus improving the photocurrent density. Besides, it can also be found that in the 6-h operation, the photocurrent densities at each light intensity operation all showed relatively excellent stability. Such good stability means the developed μVPEC is able to operate stably and efficiently, which is of importance in the real applications. In addition, the conversion rate of VO^{2+} to VO_2^+ was also calculated by the measured photocurrent at different light intensities. The calculation formula are as follows,

$$Q = \int_0^T I\mathrm{d}t \tag{5}$$

$$q = Q / (T \cdot F) \tag{6}$$

where Q (C) is the total charge in the operation period, I (A) is the current, q (mol/h) is the conversion rate, T (h) is the reaction time and F is the Faraday´s constant.

The calculated results are shown in Fig. 7b. The conversion rate of VO^{2+} was increased with the increase of the light intensity because increasing the light intensity can generate more electro-hole pairs for the photoelectrochemical oxidation of VO^{2+} to VO_2^+.

3.6 Effect of the vanadium ion concentration

In this section, the effects of the VO^{2+} and V^{3+} ion concentrations on the performance were presented. Similarly, the Nafion 115 membrane was employed. The light intensity was maintained at 130 mW/cm^2 and the flow rates were kept at 50 μL/min. To study the effect of the VO^{2+} and V^{3+} ion concentrations, the VO^{2+} and V^{3+} ion concentrations at the photoanode and cathode were the same and changed simultaneously. Both of them varied from 10.0 mM to 100.0 mM. As shown in Fig. 8a, the photocurrent density increased from 0.027 mA/cm^2 to 0.073 mA/cm^2. This is because increasing the vanadium ion concentration can enhance the mass transport from the bulk to the photoanode catalyst surfaces. As such, more photo-excited holes could be scavenged by the VO^{2+} ions followed by the photoelectrochemical oxidation to VO_2^+. As a result, the photoelectrochemical reaction rate at the photoanode could be enhanced to improve the photocurrent density. Similarly, the conversion rate of VO^{2+} was also calculated by the measured photocurrents at different vanadium concentrations. The result is shown in Fig. 8b. It can be seen that the conversion rate of VO^{2+} was increased from 0.9689 μmol/h to 2.7032 μmol/h.

4 Conclusions

In this study, a microfluidic all-vanadium photoelectrochemical cell was developed for the solar energy storage. This developed μVPEC was consisted of a TiO_2 photoanode, a commercial Pt electrode, two reaction microchambers separated by a proton exchange membrane. Such miniaturization design offers several advantages, including large surface-to-volume ratio, enhanced photon and mass transport, uniform light distribution, small internal cell resistance and easy flow control. The experimental results indicated that the developed μVPEC showed good photoresponse to the light illumination and stability for the long-term operation. In addition, the effects of the membrane thickness, the light intensity and vanadium ion concentration on the performance were also investigated. It was shown that with the increase of the membrane thickness, although the vanadium ion permeation through the membrane could be reduced, the transfer resistance of the proton was also increased, thereby increasing the internal cell resistance and decreasing the photocurrent density. Increasing the light intensity could generate more photo-excited electron-hole pairs, which could enhance the photoelectrochemical reaction rate and improve both the photocurrent density and the conversion rate. As for the effect of the vanadium ion concentration, it was found that the increase of the vanadium ion concentration could enhance the mass transport from the bulk to the photoanode catalyst surfaces, allowing more photo-excited holes to be scavenged by the VO^{2+} ions and enhancing the photoelectrochemical reaction rate. Therefore, both the photocurrent density and the conversion rate could be improved. This work not only demonstrates the

feasibility of the developed μVPEC for the solar energy storage but also provides a guidance for the optimization of this new type photoelectrochemical cell.

Acknowledgements

The authors gratefully acknowledge the financial supports of the National Natural Science Foundation of China (No. 51576021, No. 51325602 and No. 51506039).

References

[1] T. S. Zhao, L. An, L. Wei, C. Zhang, The use of polybenzimidazole membranes in vanadium redox flow batteries leading to increased coulombic efficiency and cycling performance, Electrochimica Acta, 153 (2015) 492–498.

[2] G. L. Soloveichik, Battery technologies for large-scale stationary energy storage, Annual Review of Chemical and Biomolecular Engineering, 2 (2011) 503–527.

[3] Z. G. Yang, J. L. Zhang, M. C. W. Kintner, X. C. Lu, D. W. Choi, J. P. Lemmon, J. Liu, Electrochemical Energy Storage for Green Grid, Chemical Reviews, 111 (2011) 3577–3613.

[4] C. Ponce de León, A. Frías-Ferrer, J. González-García, D. A. Szánto, F. C. Walsh, Redox flow cells for energy conversion, Journal of Power Sources, 160 (2006)

716–732.

[5] H. J. Lee, N. H. Choi, H. Kim, Analysis of concentration polarization using UV-visible spectrophotometry in a vanadium redox flow battery, Journal of the Electrochemical Society, 161 (2014) 1291–1296.

[6] H. E. S. Fath, Technical assessment of solar thermal energy storage technologies, Renewable Energy, 14 (1998) 35-40.

[7] A. A. Al-Ugla, M. A. I. El-Shaarawi, S. A. M. Said, A. M. A. Qutub, Techno-economic analysis of solar-assisted air-conditioning systems for commercial buildings in Saudi Arabia, Renewable & Sustainable Energy Reviews, 54 (2016) 1301-1310.

[8] L. L. Chen, J. Liu, X. M. Fang, Z. G. Zhang, Reduced graphene oxide dispersed nanofluids with improved photo-thermal conversion performance for direct absorption solar collectors, Solar Energy Materials & Solar Cells, 163 (2017) 125-133.

[9] M. J. Chen M, Y. R. He, J. Huang, J. Q. Zhu, Investigation into Au nanofluids for solar photothermal conversion, International Journal of Heat & Mass Transfer, 108 (2017) 1894-1900.

[10] A. Dominguez-Ramos, M. Held, R. Aldaco, M. Fischer, A. Irabien, Prospective CO2 emissions from energy supplying systems: photovoltaic systems and conventional grid within Spanish frame conditions, International Journal of Life Cycle Assessment, 15 (2010) 557-566.

[11] Z. B. Wang, Y. Y. Lin, R. Chen, Q. Liao, X. Zhu, L. An, X. F. He, W. Zhang, A

micro membrane-less photoelectrochemical cell for hydrogen and electricity generation in the presence of methanol, Electrochimica Acta, 245 (2017) 549-560.

[12] O. Brummel, F. Waidhas, U. Bauer, Y. L. Wu, S. Bochmann, H. P. Steinruck, Photochemical energy storage and electrochemically triggered energy release in the norbornadiene-quadricyclane system: UV-photochemistry and IR-spectroelectrochemistry in a combined experiment, Journal of Physical Chemistry Letters, 8 (2017) 2819-2825.

[13] J. W. Sun, X. F. Li, X. L. Xi, Q. Z. Lai, T. Liu, H. M. Zhang, The transfer behavior of different ions across anion and cation exchange membranes under vanadium flow battery medium, Journal of Power Sources, 271 (2014) 1-7.

[14] M. Skyllaskazacos, M. Rychcik, R. G Robins, A. G. Fane, M. A, Green, New all-vanadium redox flow cell, Journal of the Electrochemical Society, 133 (1986) 1057-1058.

[15] M. Skyllas-Kazacos, L. Goh, Modeling of vanadium ion diffusion across the ion exchange membrane in the vanadium redox battery, Journal of Membrane Science, 39 (2012) 43-48.

[16] M. Skyllas-Kazacos, M. Kazacos, State of charge monitoring methods for vanadium redox flow battery control, Journal of Power Sources 196 (2011) 8822-8827.

[17] C. Fujimoto, S. Kim, R. Stains, X. L. Wei, L. Y. Li, Z. G. Yang, Vanadium redox flow battery efficiency and durability studies of sulfonated Diels Alder

poly(phenylene)s, Electrochemistry Communications, 20 (2012) 48-51.

[18] W. H. Wang, X. D. Wang, Investigation of Ir-modified carbon felt as the positive electrode of an all-vanadium redox flow battery, Electrochimica Acta, 52 (2007) 6755-6762.

[19] L. Y. Li, S. Kim, W. Wang, M. Vijayakumar, Z. M. Nie, B. W. Chen, J. L. Zhang, G. G. Xia, J. Z. Hu, G. Graff, J. Liu, Z. G. Yang, Large-scale energy storage: a stable vanadium redox-flow battery with high energy density for large-scale energy storage, Advanced Energy Materials, 1 (2011) 306-306.

[20] Z. Wei, D. Liu, C. J. Hsu, F. Q. Liu, All-vanadium redox photoelectrochemical cell: An approach to store solar energy, Electrochemistry Communications, 45 (2014) 79-82.

[21] D. Liu, Z. Wei, C. J. Hsu, Y. Shen, F. Q. Liu, Efficient solar energy storage using a TiO_2/WO_3 tandem photoelectrode in an all-vanadium photoelectrochemical cell, Electrochimica Acta, 136 (2014) 435-441.

[22] D. Liu, Z. Wei, Y. Shen, S. D. Sajjad, Y. W. Hao, F. Q. Liu, Ultra-long electron lifetime induced efficient solar energy storage by an all-vanadium photoelectrochemical storage cell using methanesulfonic acid, Journal of Materials Chemistry A, 3 (2015) 20322-20329.

[23] D. Liu, Z. Wei, S. D. Sajjad, C. J. Hsu, Y. Shen, M. S. Wei, F. Q. Liu, Reversible electron storage in an all-vanadium photoelectrochemical storage cell: synergy between vanadium redox and hybrid photocatalyst, ACS Catalysis, 5 (2015) 2632-2639.

[24] R. Chen, X. Cheng, X. Zhu, Q. Liao, L. An, D. D. Ye, X. F. He, Z. B. Wang, High-performance optofluidic membrane microreactor with a mesoporous CdS/TiO_2 /SBA-15@carbon paper composite membrane for the CO_2, photoreduction, Chemical Engineering Journal, 316 (2017) 911-918.

[25] X. Cheng, R. Chen, X. Zhu, Q. Liao, X. F. He, S. Z. Li, L. Li, Optofluidic membrane microreactor for photocatalytic reduction of CO_2, International Journal of Hydrogen Energy, 41 (2016) 2457-2465.

[26] M. Xia, R. Chen, X. Zhu, Q. Liao, L. An, Z. B. Wang, X. F. He, L. Jiao, A micro photocatalytic fuel cell with an air-breathing, membraneless and monolithic design, Science Bulletin, 21 (2016) 1699-1710.

[27] L. Li, G.Y. Wang, R. Chen, X. Zhu, H. Wang, Q. Liao, Y. X. Yu, Optofluidics based micro-photocatalytic fuel cell for efficient wastewater treatment and electricity generation, Lab on a Chip, 14 (2014) 3368-3375.

[28] L. Li, R. Chen, X. Zhu, Q. Liao, H. Wang, L. An, M. Zhang, A cascading gradient pore microstructured photoanode with enhanced photoelectrochemical and photocatalytic activities, Journal of Catalysis, 344 (2016) 411–419.

[29] L. Li, S. Xue, R. Chen, Q. Liao, X. Zhu, Z.B. Wang, X.F. He, H. Feng, X. Cheng, Performance characteristics of a membraneless solar responsive photocatalytic fuel cell with an air-breathing cathode under different fuels and electrolytes and air conditions, Electrochimica Acta, 182 (2015) 280–288.

[30] N. Balis, V. Dracopoulos, M. Antoniadou, P. Lianos, Solid-state dye-sensitized solar cells made of multilayer nanocrystalline titania and poly (3-

hexylthiophene), Journal of Photochemistry & Photobiology A Chemistry, 214 (2010) 69–73.

[31] Z. Tang, D. S. Aaron, A. B. Papandrew, T. A. Z. Jr, Monitoring the state of charge of operating vanadium redox flow batteries, ECS Transactions, 41 (2012) 1-9.

[32] R. P. Brooker, C. J. Bell, L. J. Bonville, H. R. Kunz, J. M. Fenton, Determining vanadium concentrations using the UV-Vis response method, Journal of the Electrochemical Society, 162 (2015) A608-A613.

[33] L. Liu, J. Y. Xi, Z. H. Wu, W. G. Zhang, State of charge monitoring for vanadium redox flow batteries by the transmission spectra of V(IV)/V(V) electrolytes, Journal of Applied Electrochemistry, 42 (2012) 1025-1031.

Figure captions

Figure 1 Schematic diagram of (a) the μVPEC and (b) the experimental system.

Figure 2 FESEM images of the bottom dense layer: (a) top-view and (b) cross-sectional view, and the top porous layer: (c) top-view and (d) cross-sectional view.

Figure 3 The XRD pattern of the TiO_2 film.

Figure 4 Photoresponse behavior of the μVPEC. Light intensity: 130 mW/cm^2; VO^{2+} and V^{3+} concentrations: 100.0 mM; Nafion 115; Flow rate: 50 μL/min.

Figure 5 Effect of the membrane thickness: (a) the VO^{2+} permeation ratio with various membrane thicknesses (The inserted figure shows the absorbance of the VO^{2+}); (b) the variation of the photocurrent density with the membrane thickness. Light intensity: 130 mW/cm^2; VO^{2+} and V^{3+} concentrations: 100.0 mM; Flow rate: 50 μL/min.

Figure 6 EIS Nyquist plots of the μVPEC and large-scale batch reactor.

Figure 7 Effect of the light intensity: (a) the variation of the photocurrent density; (b) the variation of the conversion rate. VO^{2+} and V^{3+} concentrations: 100.0 mM; Nafion 115; Flow rate: 50 μL/min.

Figure 8 Effect of the vanadium ion concentration: (a) the change of the photocurrent density; (b) the change of the conversion rate. Light intensity: 130 mW/cm^2; Nafion 115; Flow rate: 50 μL/min.

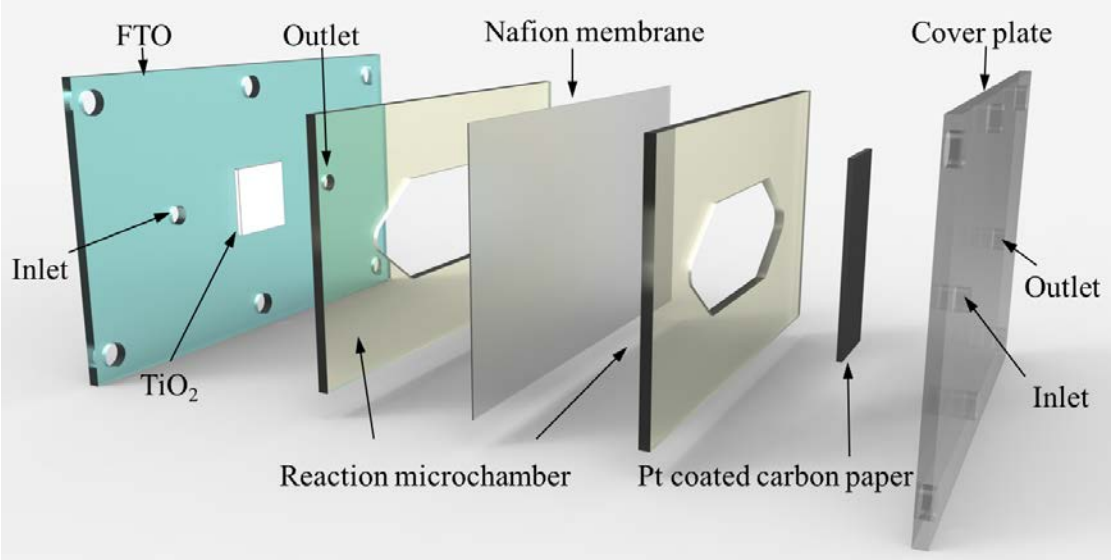

(a)

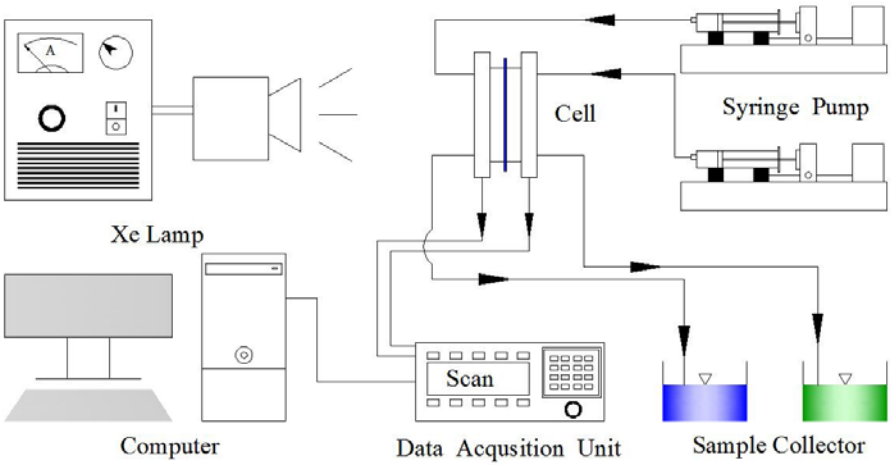

(b)

Fig. 1 Schematic diagram of (a) the μVPEC and (b) the experimental system.

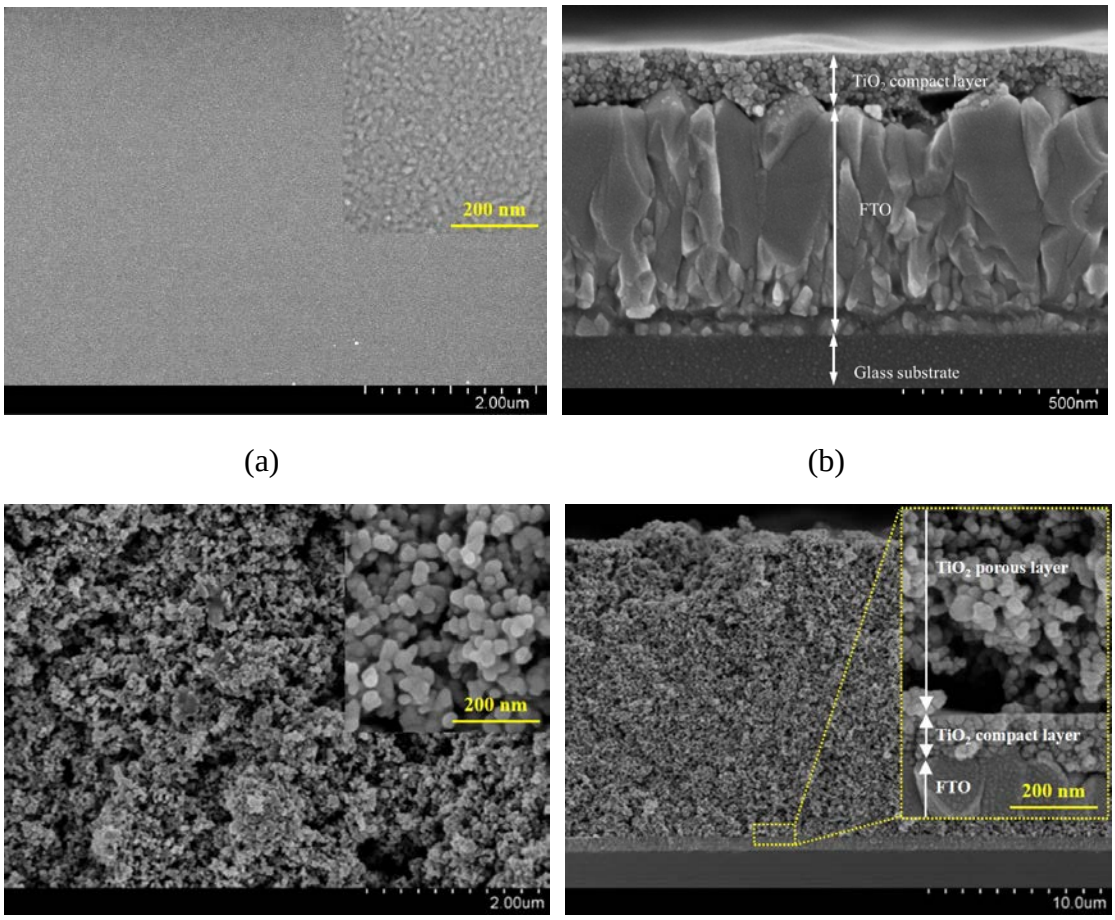

Fig. 2 FESEM images of the bottom dense layer: (a) top-view and (b) cross-sectional view, and the top porous layer: (c) top-view and (d) cross-sectional view.

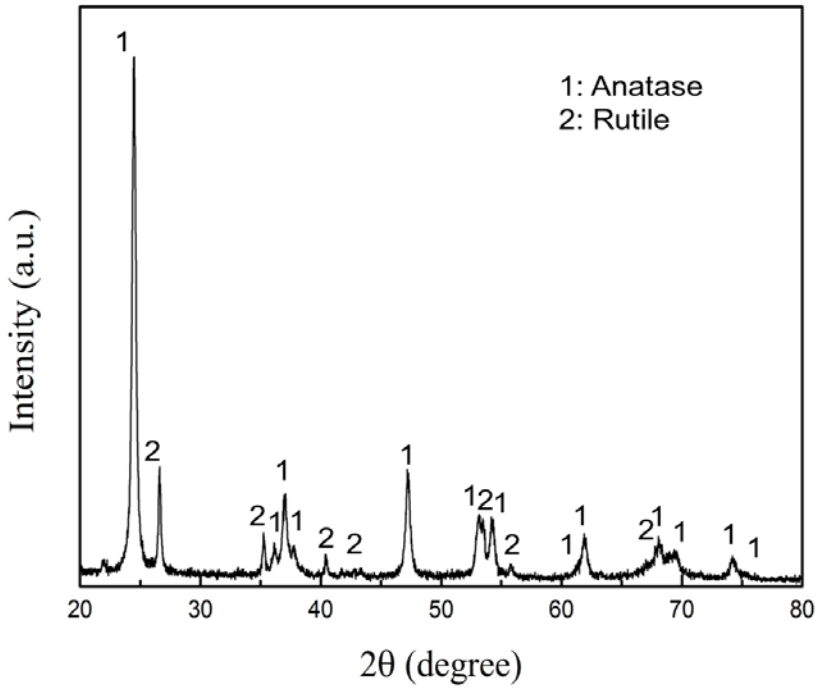

Fig. 3 The XRD pattern of the TiO_2 film.

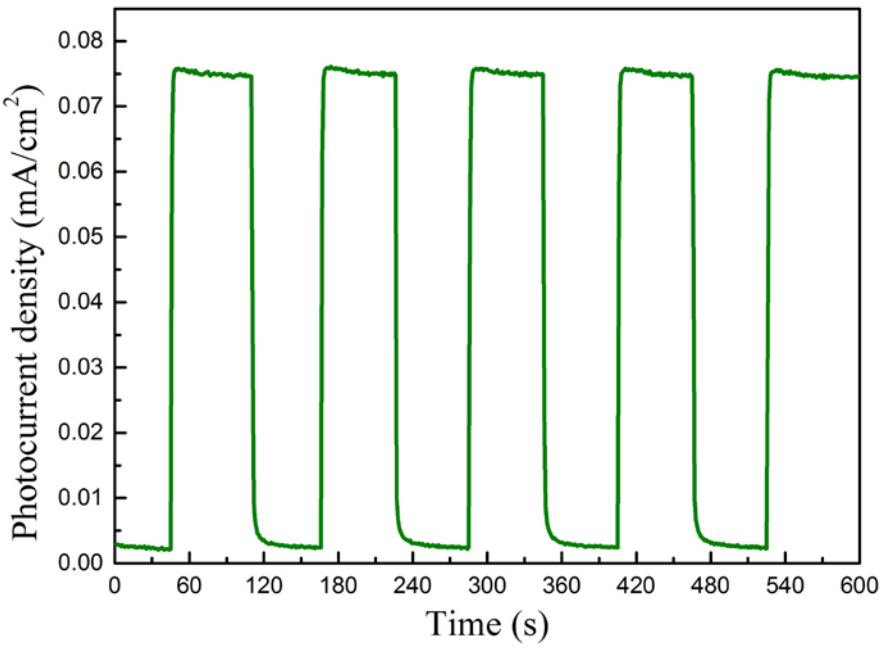

Fig. 4 Photoresponse behavior of the μVPEC. Light intensity: 130 mW/cm^2; VO^{2+} and V^{3+} concentrations: 100.0 mM; Nafion 115; Flow rate: 50 μL/min.

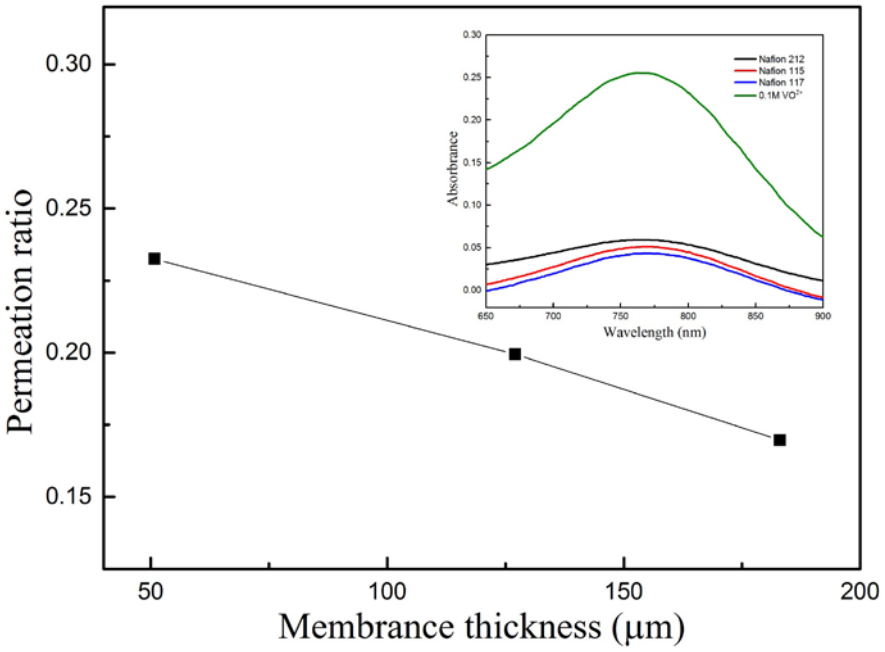

(a)

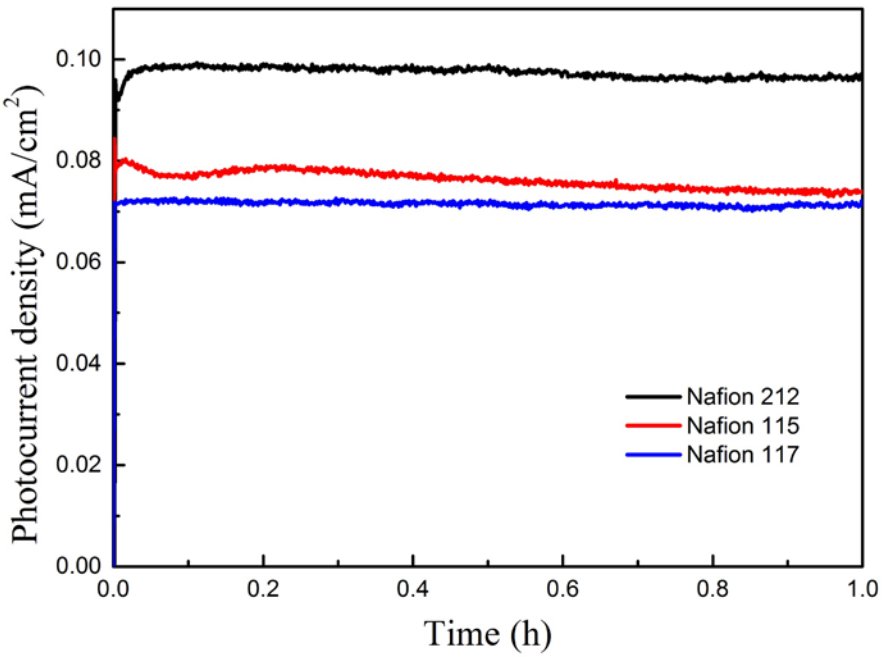

(b)

Fig. 5 Effect of the membrane thickness: (a) the VO^{2+} permeation ratio with various membrane thicknesses (The inserted figure shows the absorbance of the VO^{2+}); (b) the variation of the photocurrent density with the membrane thickness. Light intensity: 130 mW/cm^2; VO^{2+} and V^{3+} concentrations: 100.0 mM; Flow rate: 50 μL/min.

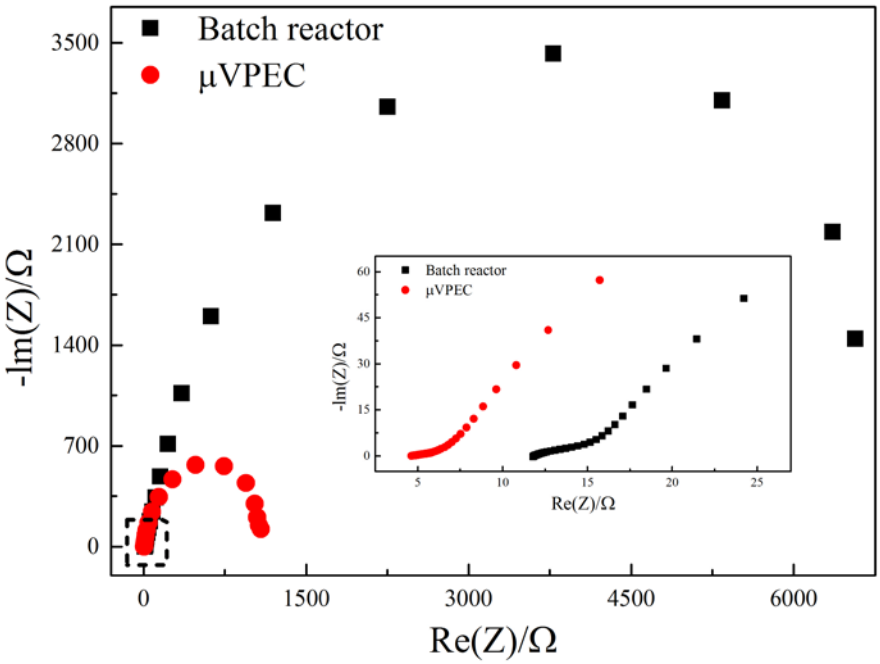

Fig. 6 EIS Nyquist plots of the μVPEC and large-scale batch reactor.

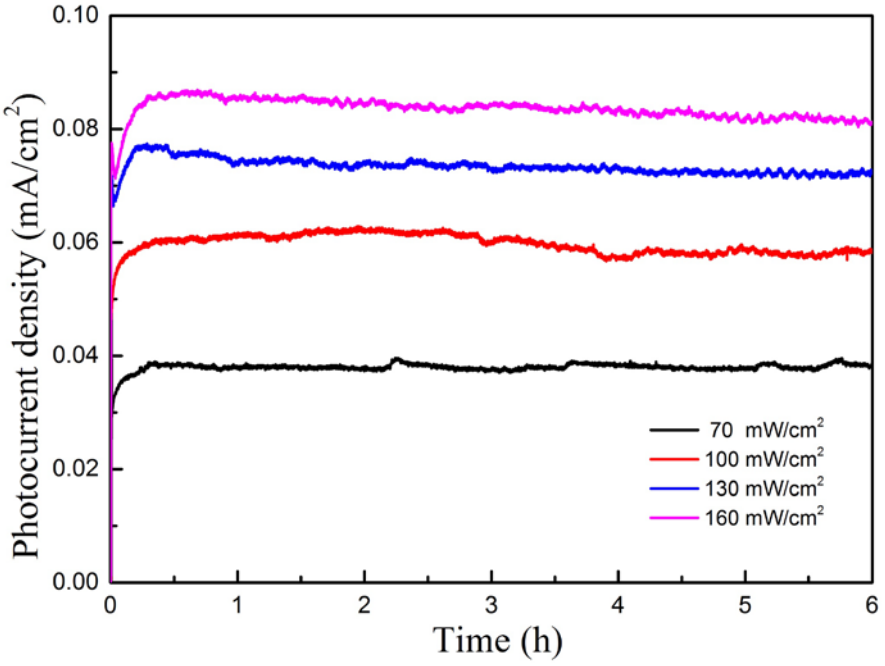

(a)

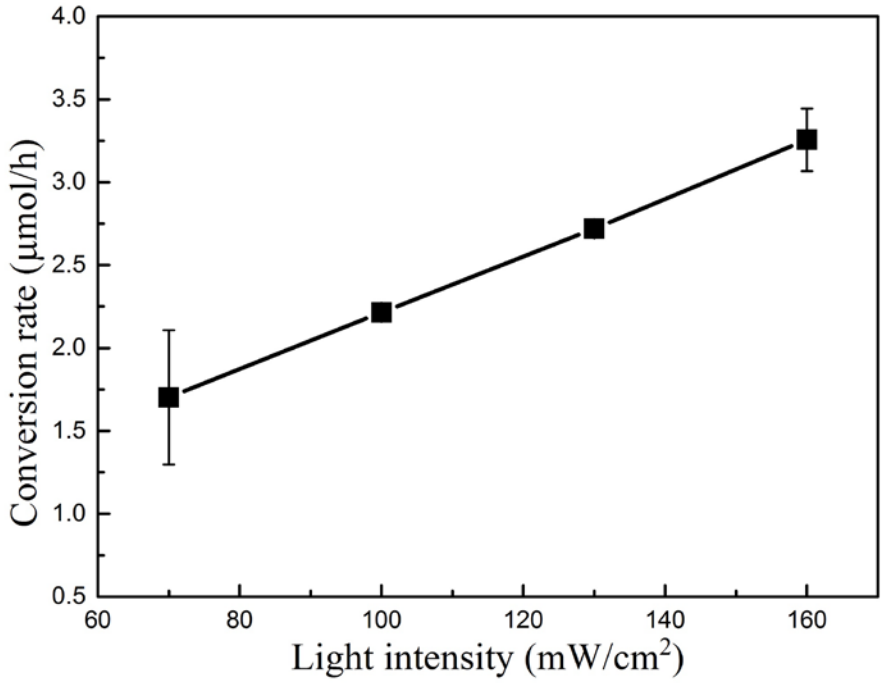

(b)

Fig. 7 Effect of the light intensity: (a) the variation of the photocurrent density; (b) the variation of the conversion rate. VO^{2+} and V^{3+} concentrations: 100.0 mM; Nafion 115; Flow rate: 50 μL/min.

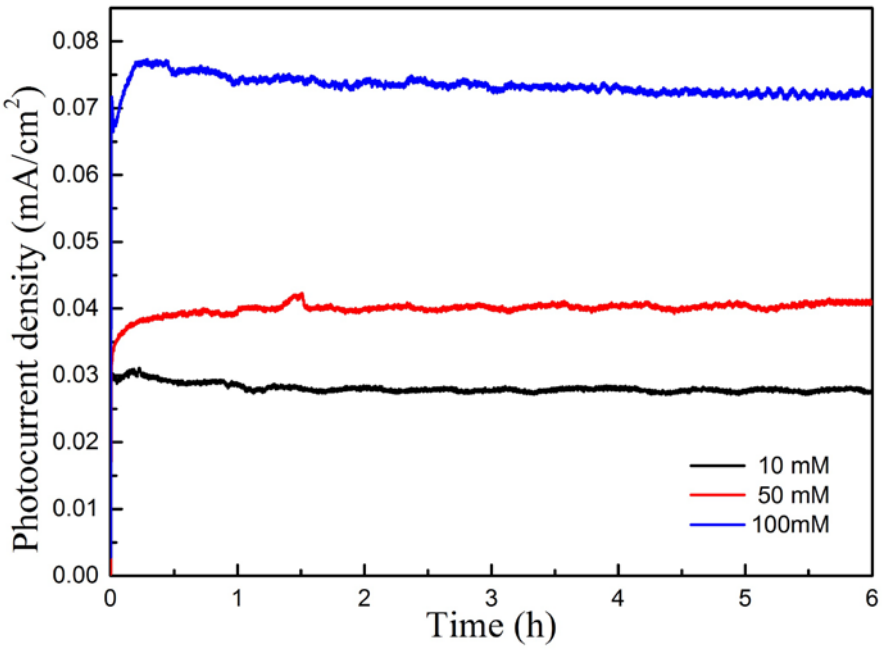

(a)

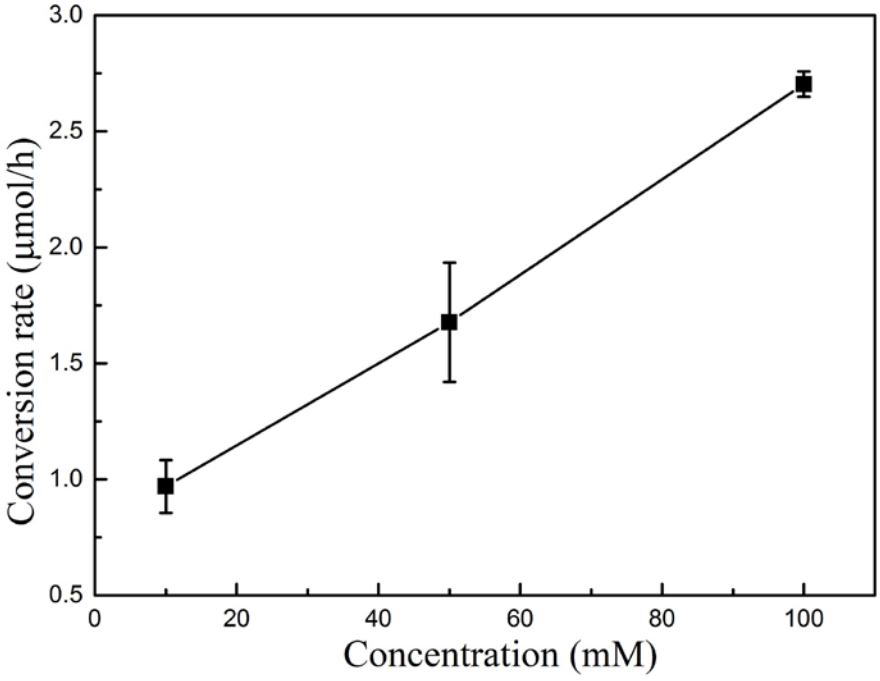

(b)

Fig. 8 Effect of the vanadium ion concentration: (a) the change of the photocurrent density; (b) the change of the conversion rate. Light intensity: 130 mW/cm^2; Nafion 115; Flow rate: 50 μL/min.